Neuron, Vol. 31, 973–985, September 27, 2001, Copyright ©2001 by Cell Press

Preassociation of Calmodulin with Voltage-Gated Ca^{2+} Channels Revealed by FRET in Single Living Cells

Michael G. Erickson,[1] Badr A. Alseikhan,[1] Blaise Z. Peterson,[2] and David T. Yue[1,3]
[1]Department of Biomedical Engineering and Department of Neuroscience
Calcium Signals Laboratory
Johns Hopkins University School of Medicine
Baltimore, Maryland 21205
[2]Department of Cellular and Molecular Physiology
College of Medicine
Pennsylvania State University
Hershey, Pennsylvania 17033

Summary

Among the most intriguing forms of Ca^{2+} channel modulation is the regulation of L-type and P/Q-type channels by intracellular Ca^{2+}, acting via unconventional channel-calmodulin (CaM) interactions. In particular, overexpressing Ca^{2+}-insensitive mutant CaM abolishes Ca^{2+}-dependent modulation, hinting that Ca^{2+}-free CaM may "preassociate" with these channels to enhance detection of local Ca^{2+}. Despite the far-reaching consequences of this proposal, in vitro experiments testing for preassociation provide conflicting results. Here, we develop a three filter-cube fluorescence resonance energy transfer method (three-cube FRET) to directly probe for constitutive associations between channel subunits and CaM in single living cells. This FRET assay detects Ca^{2+}-independent associations between CaM and the pore-forming α_1 subunit of L-type, P/Q-type, and, surprisingly, R-type channels. These results now definitively demonstrate channel-CaM preassociation in resting cells and underscore the potential of three-cube FRET for probing protein-protein interactions.

Introduction

An unusual twist to the classic view of calmodulin is that Ca^{2+}-free CaM (apoCaM) sometimes preassociates with a target molecule, whose activity is subsequently modulated when Ca^{2+}-CaM shifts to another site on the target (Jurado et al., 1999). Representative examples of this intriguing phenomenon include apoCaM interaction with the skeletal muscle ryanodine receptor (Rodney et al., 2000) and small-conductance Ca^{2+}-activated K^+ channel (Xia et al., 1998).

Recent studies reveal that Ca^{2+}-dependent regulation of gating in both L-type (α_{1C}) and P/Q-type (α_{1A}) Ca^{2+} channels is mediated by interaction of Ca^{2+}-activated CaM with the carboxyl tail of respective α_1 pore-forming subunits (DeMaria et al., 2001; Lee et al., 1999; Peterson et al., 1999; Qin et al., 1999; Zuhlke et al., 1999). In addition, there are tantalizing clues from these reports that CaM may be preassociated with the L-type (Peterson et al., 1999; Zuhlke et al., 1999) and P/Q-type (DeMaria et al., 2001) channel complexes, even before the influx of Ca^{2+}. When expressed alone in heterologous systems, these channels modulate normally (Peterson et al., 1999, and unpublished data), indicating that there are sufficient quantities of endogenous CaM. However, Ca^{2+}-dependent modulation in both channel types is completely eliminated by coexpressing a Ca^{2+}-insensitive mutant CaM (CaM_{MUT}) with alanine substitutions in the first ligand position of all four EF hands (DeMaria et al., 2001; Peterson et al., 1999). The dominant-negative knockout of Ca^{2+}-dependent modulation by CaM_{MUT} could signify that CaM preassociates, since CaM_{MUT} appears to block endogenous CaM from accessing the Ca^{2+}-CaM effector site on the α_1 subunit (DeMaria et al., 2001; Peterson et al., 1999; Zuhlke et al., 1999). Such preassociation generally ensures selective responsiveness to local Ca^{2+} (Jurado et al., 1999). If true in the case of Ca^{2+} channels, preassociation would be an effective means of enabling accelerated modulation by local Ca^{2+} influx.

Despite these exciting implications, it has not yet been possible to exclude other equally plausible explanations for the dominant-negative behavior of CaM_{MUT}, such as downregulation of endogenous CaM by overexpression of CaM_{MUT}. Furthermore, attempts to test for preassociation in vitro have yielded contradictory results. These efforts have focused predominantly on the proximal third of the α_{1C} carboxyl tail, which encompasses structures in the CI region (Figure 1A) known to be important for Ca^{2+}-dependent inactivation (de Leon et al., 1995; Peterson et al., 1999, 2000; Soldatov et al., 1997; Zhou et al., 1997; Zuhlke and Reuter, 1998). Recent investigations along these lines have found evidence for in vitro binding of CaM to the CI region in zero to minimal concentrations of Ca^{2+} (50–100 nM) normally present in resting cells (Pitt et al., 2001; Romanin et al., 2000). However, separate investigations using the same or similar techniques yielded directly conflicting results (Ivanina et al., 2000; Pate et al., 2000; Peterson et al., 1999). The many discrepancies among these reports raise questions as to whether the interactions actually occur in living cells. Our conception of preassociation with P/Q-type channels is similarly clouded, since CaM_{MUT} eliminates Ca^{2+}-dependent modulation of these channels (DeMaria et al., 2001), yet, only in the presence of Ca^{2+} did CaM coprecipitate with the α_{1A} carboxyl tail (Peterson et al., 1999) or full-length α_{1A} (Lee et al., 1999).

What accounts for these conflicting results? It could be that the primary locus for CaM preassociation with the channel complex resides outside of the pore-forming α_1 subunit, such as on the accessory β subunit. Alternatively, the reported disagreements may reflect fundamental challenges in identifying a genuine apoCaM binding site (Jurado et al., 1999). It is possible that in vitro detection of the interactions supporting apoCaM preassociation is severely compromised by denaturing conditions required to solubilize the channel or channel fragments. High-affinity apoCaM binding pockets may be especially susceptible to such disruption because their formation can require synergistic alignment of multiple, nonadjoining ligand segments. These segments may in-

[3]Correspondence: dyue@bme.jhu.edu

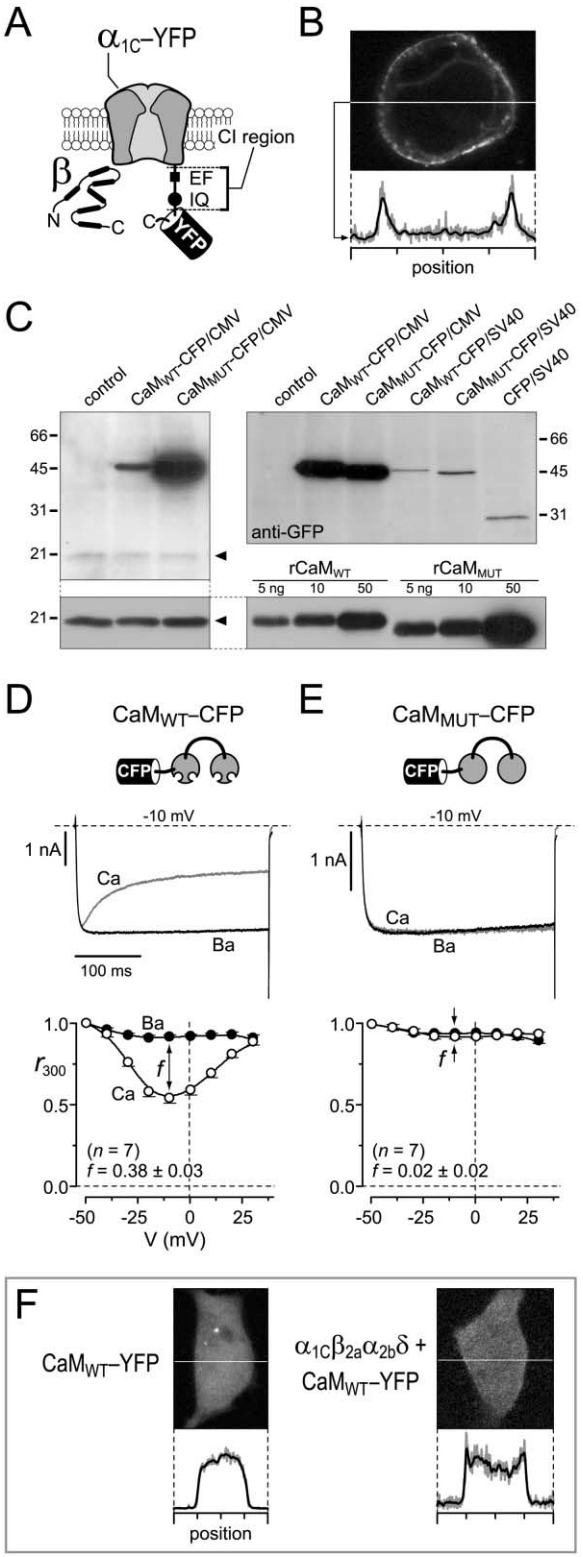

Figure 1. CaM_{WT}-CFP and α_{1C}-YFP Preserve Ca^{2+}-Dependent Inactivation

(A) α_{1C}-YFP, showing β_{2a} subunit and CI region (Peterson et al., 1999).

(B) Confocal image and intensity profile for cell expressing α_{1C}-YFP/$\beta_{2a}/\alpha_{2b}\delta$; peaks indicate membrane targeting.

(C) Immunoblots of HEK293 lysates probed with anti-CaM or anti-GFP (labeled) antibodies. Upper left, comparison of control (mock transfected) cells with cells overexpressing CaM_{WT}-CFP or CaM_{MUT}-CFP, arrowhead indicates endogenous CaM at ~20 kDa. Lower left, same lysates as above, optimized for visualization of endogenous CaM (see Experimental Procedures), showing that endogenous CaM expression is unchanged. Lower right, calibration ladder for purified recombinant CaM_{WT} and CaM_{MUT}, conditions same as at left. Upper right, immunoblot probed with anti-GFP antibody comparing CMV and SV40 promoter systems.

(D) Whole-cell currents from cells coexpressing α_{1C}-YFP/$\beta_{2a}/\alpha_{2b}\delta$ and CaM_{WT}-CFP. Upper, exemplar Ba^{2+} (black) and scaled Ca^{2+} (gray) currents during depolarizing steps to –10mV. Lower, fraction of current remaining at the end of 300 ms depolarizations (r_{300}).

(E) Results from cells coexpressing α_{1C}-YFP/$\beta_{2a}/\alpha_{2b}\delta$ and CaM_{MUT}-CFP, format identical to (D).

(F) Confocal images and intensity profiles for cells expressing CaM_{WT}-YFP alone (left) or together with $\alpha_{1C}/\beta_{2a}/\alpha_{2b}\delta$ (right), showing some perimembrane enrichment of CaM_{WT}-YFP (peaks in intensity profile) when coexpressed with unlabeled channels.

dividually manifest only weak interaction with apoCaM, as in the cases of glycogen phosphorylase b kinase and *Bordetella pertussis* adenyl cyclase (Jurado et al., 1999). Precedence for this idea in the realm of ion channels can be drawn from the small-conductance Ca^{2+}-activated K^+ channel, in which the carboxyl lobe of CaM binds to two noncontiguous helical segments in a Ca^{2+}-independent manner (Schumacher et al., 2001).

Here, we apply assays based on FRET (Selvin, 1995) between GFP color mutants (Miyawaki et al., 1997) CFP and YFP to obviate such concerns and investigate directly apoCaM interactions in the setting of ultimate relevance—living cells. This general strategy has been successfully employed in recent investigations of receptor-mediated activation of G proteins (Janetopoulos et al., 2001), calpain signaling in presynaptic termini (Vanderklish et al., 2000), and preassociation of Fas receptors (Siegel et al., 2000). In the present study, CFP and YFP are fused to CaM and a target Ca^{2+} channel protein such that constitutive association of CaM with the target tends to bring CFP and YFP within 100 Å, leading to nonradiative energy transfer to YFP and its sensitized green-yellow emission. Using this approach applied to single resting cells, we uncover significant, Ca^{2+}-independent associations between CaM (or CaM_{MUT}) and L-type, P/Q-type, and, unexpectedly, R-type (α_{1E}) Ca^{2+} channels. Calmodulin appears to be preassociated with each channel type at the same relative location, although the binding affinities differ substantially. Based on differences in the FRET coupling among labeled Ca^{2+} channel subunits and CaM, we hypothesize the arrangement of key constituents of a complete L-type channel complex, although this coarse mapping is limited by several key assumptions (see Discussion). Overall, these findings provide the first definitive evidence for CaM preassociation with voltage-gated Ca^{2+} channels in living cells and illustrate the general utility of three-cube FRET for exploring the many remaining prospective apoCaM-target interactions (Rhoads and Friedberg, 1997).

Results

Fusing GFP Variants to α_{1C} and CaM Preserves Ca^{2+}-Dependent Inactivation

Key prerequisites for our experiments were strategic attachment of CFP/YFP and verification that the re-

sulting fusion proteins preserved the interactions in question. Focusing on L-type channels, CaM mediates feedback inhibition of channel opening by elevated intracellular Ca^{2+} (Ca^{2+}-dependent inactivation [Brehm and Eckert, 1978]). Two CaM-channel interactions figure importantly: (1) inferred preassociation of apoCaM with the channel complex, at a presently uncertain site (Peterson et al., 1999; Zuhlke et al., 1999), and (2) initiation of inactivation by Ca^{2+}-CaM binding to the IQ-like domain on the proximal carboxyl tail of the pore-forming α_{1C} subunit (Peterson et al., 1999; Qin et al., 1999; Zuhlke et al., 1999) (Figure 1A). In designing the fusion of YFP to the channel, we suspected that if apoCaM indeed preassociates with the channel complex, it would be close to the IQ site. We therefore truncated the α_{1C} carboxyl tail just beyond the IQ site before fusion to YFP (Figure 1A, α_{1C}-YFP), so as to favor FRET detection of apoCaM association. CFP was fused to the amino lobe of CaM_{WT} and CaM_{MUT}, yielding CaM_{WT}-CFP and CaM_{MUT}-CFP.

The remainder of Figure 1 (1B–1F) establishes that these fusion constructs preserved the functional interactions underlying Ca^{2+}-dependent inactivation. HEK293 cells expressing labeled L-type channels (α_{1C}-YFP/β_{2a}/$\alpha_{2b}\delta$) displayed a distinct fluorescent ring at the cell perimeter (Figure 1B) and had substantial recombinant currents (below), confirming that labeled channels are functional and properly target the plasma membrane. Western blots (Figure 1C), from HEK293 cells transfected with CaM_{WT}-CFP or CaM_{MUT}-CFP, showed strong expression of labeled CaMs and no cleavage of linked CFP. Coexpression of labeled channels with CaM_{WT}-CFP resulted in whole-cell currents with robust Ca^{2+}-dependent inactivation (Figure 1D), as the sharp decay of Ca^{2+} current shows (gray trace). The corresponding Ba^{2+} current (black trace) inactivated little, as expected from the high Ca^{2+} selectivity of CaM (Chao et al., 1984). Averages from multiple cells verified uniformly strong Ca^{2+}-dependent inactivation (Figure 1D, lower), as gauged by the fraction of peak current remaining at the end of 300 ms voltage steps (r_{300}) (de Leon et al., 1995). The difference between Ca^{2+} and Ba^{2+} relations (f) quantifies pure Ca^{2+}-dependent inactivation. These results closely matched those for unlabeled channels (α_{1C}/β_{2a}/$\alpha_{2b}\delta$) (Peterson et al., 2000), indicating that labeled constructs preserved Ca^{2+}-dependent inactivation and, by inference, the underlying Ca^{2+}-CaM/IQ interaction. In contrast, coexpressing labeled channels with CaM_{MUT}-CFP, which mimics apoCaM (Xia et al., 1998), ablated Ca^{2+}-dependent inactivation (Figure 1E), matching results for coexpression of untagged channels and CaM_{MUT} (Peterson et al., 1999). Importantly, the elimination of inactivation by CaM_{MUT}-CFP was not due to downregulation of endogenous CaM (Figure 1C, arrowhead), which was unchanged with overexpression of CFP-tagged CaMs. Thus, labeling of CaM and channels preserved the dominant-negative behavior suggesting apoCaM interaction (Peterson et al., 1999; Zuhlke et al., 1999).

Given that L-type channels robustly target the plasma membrane (Figure 1B), one might predict that CaM preassociation would result in elevated concentrations of CaM near the membrane. To test this hunch, we collected confocal images of cells expressing CaM_{WT}-YFP both in the absence and presence of unlabeled channels (Figure 1F). Small peaks in the image profile corresponding to perimembrane enrichment of CaM_{WT}-YFP were apparent only with coexpression of L-type channels. Though far from definitive, such preferential enrichment encouraged us to undertake direct, FRET-based tests for preassociation, as described below.

Sensitive and Selective Detection of FRET in Living Cells Using Three-Cube FRET

While CFP and YFP fusion constructs solved the problem of producing functional and specifically labeled CaM and channels, measuring steady-state FRET was complicated by both variability in recombinant expression and the inability to selectively excite CFP. We therefore developed a convenient, microscope-based three-cube FRET assay for sensitized YFP emission that controls for these problems and normalizes out the inevitable small aberrations of actual optical components.

To understand the principles of three-cube FRET, consider the fluorescence emission spectrum (Figure 2A) produced by illuminating both CFP and YFP with light at 440 nm. The double-humped shape results from superposition of underlying CFP and YFP spectra. FRET alters this spectrum by decreasing the CFP (donor) peak near 480 nm and enhancing the YFP (acceptor) peak near 535 nm (Miyawaki et al., 1997). FRET can be nondestructively quantified by enhanced YFP emission, provided we can dissect the sources of emission at 535 nm. Although general methods for such optical dissection have been established (Clegg, 1992; Gordon et al., 1998; Tron et al., 1984), three-cube FRET accomplishes this objective while exploiting simplifications made possible by the spectral properties of CFP and YFP.

Emission at 535 nm (Figure 2A, number 1) is the sum of CFP emission (number 2) and YFP emission (number 3), a portion of which is due to direct excitation (number 4). To dissect these components, three-cube FRET employs filter cubes that isolate CFP and YFP signals from a cell expressing both fluorophores. The CFP cube excites both fluorophores but measures fluorescence where only CFP emits (number 5). Multiplying this measurement by a predetermined constant provides CFP emission at 535 nm (number 2), which is subtracted from number 1 to determine total YFP emission (F_{A_D}; number 3). Similarly, the YFP cube measures near exclusive YFP emission by preferential excitation of YFP. Multiplying this measurement by a constant gives YFP emission due to direct excitation (F_{A_D}; number 4). Finally, we calculate the FRET ratio ($FR = F_{A_D}/F_A$), a unitless index equal to the fractional increase in YFP emission due to FRET. As the amount of FRET increases, FR rises above unity, reaching a theoretical maximum of ~12 if the CFP/YFP pair was to undergo FRET with 100% efficiency (E). FR bears a linear relation to the effective FRET efficiency, $E_{EFF} = E \times A_b$, where A_b is the fraction of YFP-tagged molecules that are associated with CFP-tagged molecules (equation 2, Experimental Procedures). When A_b is 1, E_{EFF} can be used to estimate the physical donor-acceptor separation, according to the Förster equation (see Experimental Procedures).

Control experiments verified that three-cube FRET provides sensitive and selective detection of FRET (Figure 2B). Averaged data from individual cells expressing only YFP gave FR ~1, as expected for this trivial case

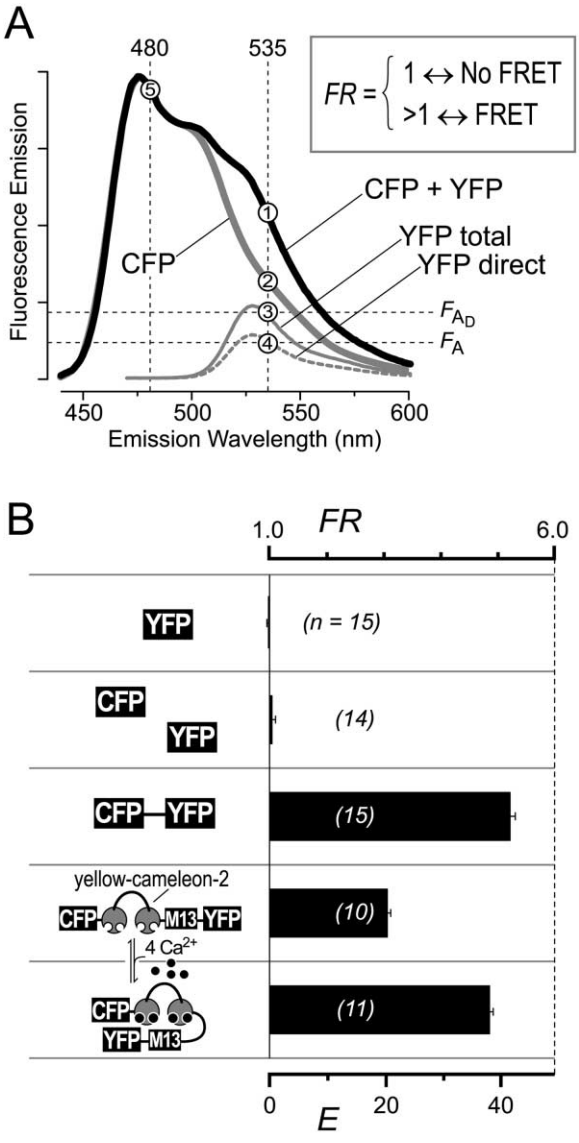

Figure 2. FRET Detection by Three-Cube FRET

(A) Dissection of 535 nm emission with 440 nm excitation. Graph, overall emission spectrum from single cell expressing CFP- and YFP-tagged proteins (black line), reflecting underlying CFP (thick gray) and YFP (thin gray) spectra. Portion of YFP emission is due to direct excitation (gray dashed). Points 1 through 5 are described in the text.

(B) Three-cube FRET control experiments on single live cells expressing indicated constructs. Horizontal axes, FRET ratio, and FRET percent efficiency (*E*). For yellow cameleon-2, cells were incubated in 10 μM ionomycin for 15 min before application of either 5 mM EGTA or 20 mM CaCl in buffered Tyrode's.

when no donor is present. Cells coexpressing CFP and YFP also showed no FRET, arguing against confounding concentration-dependent artifacts (Moon et al., 2001). A significant increase in *FR* was observed for cells expressing a CFP-YFP concatemer in which CFP and YFP are held within 100 Å. Finally, the calcium sensor yellow cameleon-2 showed the expected Ca^{2+}-dependent increase in *FR* (Miyawaki et al., 1997).

An important methodological consideration was to express all small, diffusible proteins such as CaM and CFP with a weak SV40 promoter system rather than standard strong CMV promoters (Figure 1C); otherwise, recombinant protein concentrations could be high enough to support spurious FRET (Moon et al., 2001). Channel subunits, which are far more difficult to express, remained under the control of a CMV promoter to ensure adequate signal levels. Another critical consideration was to attach YFP to the presumed limiting moiety in a given interaction, thus maximizing A_b so as to favor detection of FRET. This strategy provided the additional advantage of increasing the effective spatial resolution of our system, according to the following logic. After subtracting the contribution to the *FRET* cube reading (Figure 2A, number 1) from CFP-tagged molecules residing throughout the cell (number 2), the remaining fluorescence signal (number 3) arises solely from YFP-tagged channel subunits targetted to the plasma membrane (Figure 1B). Since this remaining YFP signal is the basis for calculating *FR*, the three-cube method selectively resolves FRET in the perimembrane region.

CaM and CaM_{MUT} Preassociate with L-Type Channels in Resting Cells

Armed with this three-cube FRET assay, we returned to investigation of apoCaM association with L-type channels (Figure 3A). Coexpressing CFP with tagged channels (α_{1C}-YFP/β_{2a}/$\alpha_{2b}\delta$) resulted in *FR* ~1, ruling out concentration-dependent FRET. In striking contrast, coexpressing CaM_{WT}-CFP with tagged channels supported a nearly 2-fold increase in YFP emission due to FRET, indicating that α_{1C}-YFP and CaM-CFP are <100 Å apart in resting cells. The characteristic change in YFP emission is illustrated by Figure 2A, in which the spectra have been scaled to correspond to a typical cell coexpressing CaM_{WT}-CFP with tagged channels. Coexpressing CaM_{MUT}-CFP with labeled channels gave an elevated *FR* indistinguishable from that observed with CaM_{WT}-CFP. Since CaM_{MUT} does not bind Ca^{2+} at intracellular levels of [Ca^{2+}] (Xia et al., 1998), this result argues strongly that CaM-channel association in resting cells involves a genuine, Ca^{2+}-independent interaction. One trivial explanation for CaM-channel colocalization would be generalized enrichment of CaM at the surface membrane, independent of CaM binding to the channel complex. This possibility was excluded by the failure of β_{2a}-YFP, which itself robustly targets the plasma membrane (Chien et al., 1995), to support FRET with CaM_{WT}-CFP in the absence of α_{1C} (Figure 3B). Moreover, coexpressing CaM_{WT}-CFP with channels labeled on the β_{2a} subunit (α_{1C}/β_{2a}-YFP/$\alpha_{2b}\delta$) restored a small but significant elevation of *FR* (Figure 3B), suggesting that CaM-channel association requires the α_{1C} subunit.

Preassociation of CaM_{MUT} with P/Q- and R-Type Channels

We next asked whether R-type (α_{1E}) or P/Q-type (α_{1A}) channels support preassociation, since α_{1E} and α_{1A} also possess homologous IQ-like domains that bind Ca^{2+}-CaM in vitro (DeMaria et al., 2001; Pate et al., 2000; Peterson et al., 1999). We therefore generated α_{1E}-YFP and α_{1A}-YFP, with carboxyl terminus truncations and YFP fusions carried out as with α_{1C}-YFP. No form of Ca^{2+}-

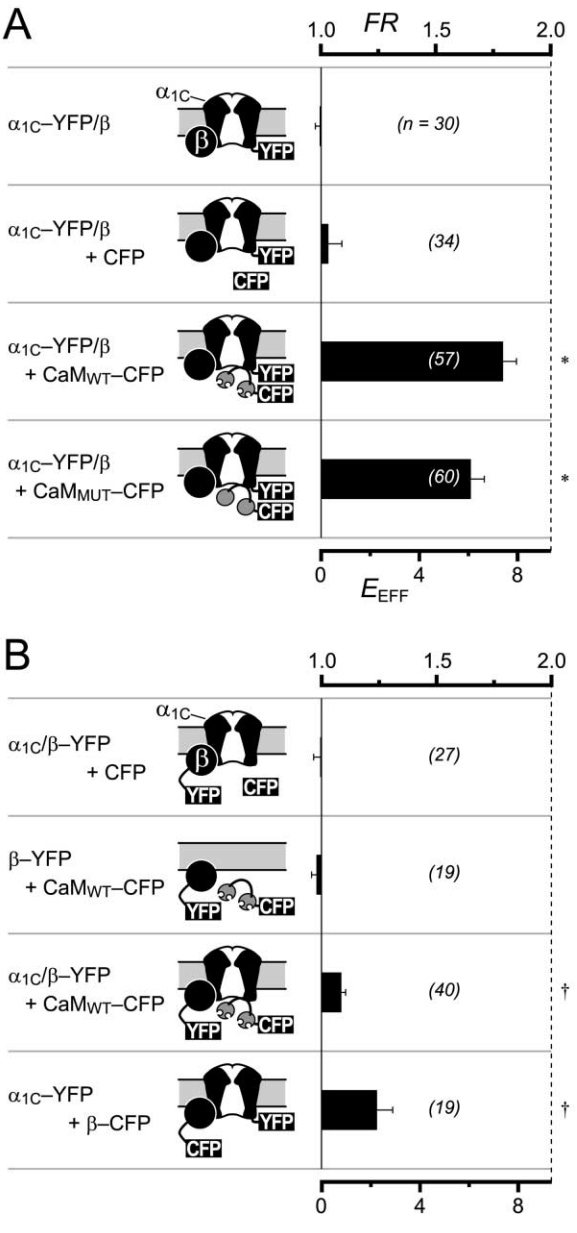

Figure 3. Preassociation of CaM with L-Type Ca^{2+} Channel Complex

(A and B) Three-cube FRET control experiments on single live cells expressing indicated constructs. Horizontal axes, *FR*, and effective FRET percent efficiency (E_{EFF}). $\alpha_{2b}\delta$ subunits also transfected.

(A) Three-cube FRET experiments reveal CaM_{WT} and CaM_{MUT} preassociation with L-type channels in resting cells. *, $p < 0.01$ versus free CFP.

(B) Preassociation with L-type channel complexes requires the α_{1C} pore-forming subunit. †, $p < 0.05$ versus free CFP.

dependent modulation of R-type gating has been described thus far. It was surprising, therefore, that coexpressing α_{1E}-YFP/β_{2a}/$\alpha_{2b}\delta$ with CaM_{MUT}-CFP supported significant FRET (Figure 4), providing direct evidence that apoCaM associates with R-type channels. Binding of Ca^{2+}-CaM to the IQ-like domain of α_{1A} is now known to be essential for Ca^{2+}-dependent modulation of P/Q-type channels (DeMaria et al., 2001). Cells coexpressing

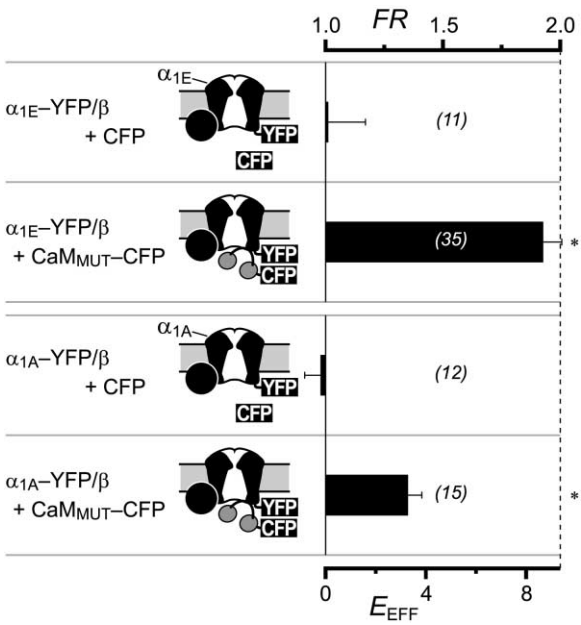

Figure 4. Preassociation of CaM with R-Type and P/Q-Type Ca^{2+} Channel Complexes

Format identical to Figure 3. $\alpha_{2b}\delta$ subunits also transfected. *, $p <$ 0.01 versus free CFP.

α_{1A}-YFP/β_{2a}/$\alpha_{2b}\delta$ with CaM_{MUT}-CFP showed clear elevation of *FR* (Figure 4), suggesting that apoCaM also associates with P/Q-type channels. Considered together, these results mark the first direct evidence that preassociation of apoCaM is a widely employed strategy among the class of high-voltage activated (HVA) Ca^{2+} channels.

Estimation of Binding Affinities and Triangulation of Major Channel Landmarks

FRET not only provides a qualitative indication of protein-protein association but in the best cases it also can be used to estimate physical distances between donor and acceptor fluorophores (Stryer and Haugland, 1967). However, this estimation requires that each YFP-tagged molecule be associated with a CFP-tagged partner. Since we intentionally limited expression of CFP-tagged moieties to avoid spurious FRET, this condition may not have been satisfied. To overcome this limitation, we developed a CaM-channel association model. Details of this model are provided in Experimental Procedures and Supplemental Appendices found at http://www.neuron.org/cgi/content/full/31/6/973/DC1. In brief, the relative numbers of CFP- and YFP-tagged molecules, N_D and N_A, were estimated using the optical isolation afforded by three-cube FRET. We then assumed a relative dissociation constant ($K_{d,EFF}$), which when combined with a 1:1 ligand binding function permitted calculation of A_b, the fraction of YFP-tagged molecules associated with CFP-tagged partners. In turn, *FR* was predicted according to the equation $FR = 1 + A_b(FR_{max} - 1)$, using an initial guess for the maximal *FR* reached when $A_b = 1(FR_{max})$. $K_{d,EFF}$ and FR_{max} can then be determined by adjusting these two parameters to achieve the best fit of the predicted *FR* values.

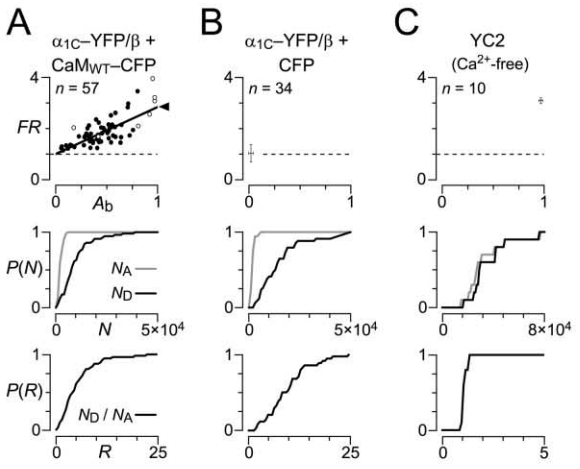

D

–YFP	–CFP	$K_{d,EFF}$	FR_{max}
α_{1C}	CaM_{WT}	9100	2.9
α_{1C}	CaM_{MUT}	6300	2.8
β_{2a}	CaM_{WT}	5800	1.2
α_{1C}	β_{2a}	43	1.2
α_{1E}	CaM_{MUT}	4800	3.5
α_{1A}	CaM_{MUT}	14000	3.0

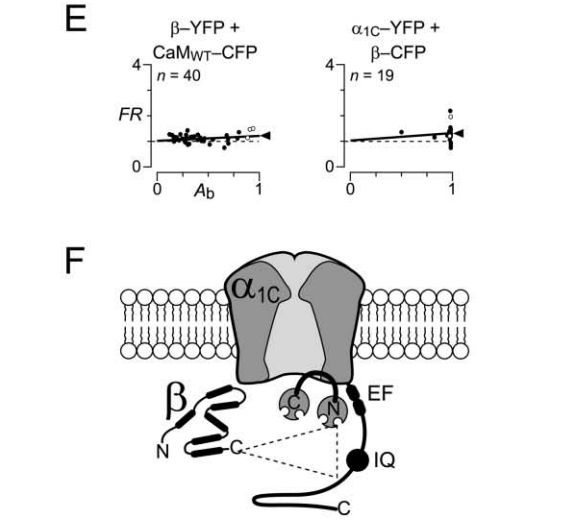

Figure 5. Model of CaM Preassociation

(A) Analysis of *FR* data for cells coexpressing CaM_{WT}-CFP and α_{1C}-YFP/β_{2a}/$\alpha_{2b}\delta$. Upper, comparison of measured (filled circles) and predicted (black line) *FR* values for cells coexpressing FRET between pairings plotted versus calculated fraction bound, A_b. Arrowhead indicates the maximal *FR*, FR_{max}. In addition to using three-cube FRET, FRET was also measured by swapping CFP and YFP and quantitating CFP dequenching following complete acceptor photodestruction (open circles; refer to equations 2 and 3 in Experimental Procedures). Middle, probability distribution function of relative number of molecules, $P(N) = Prob$(number of molecules $\leq N$). N_D (black) and N_A (gray) are relative numbers of CFP- and YFP-tagged molecules, respectively, as determined by three-cube FRET measurements (see Experimental Procedures). Lower, probability distribution function of ratio of CFP-tagged molecules to YFP-tagged molecules, $P(R) = Prob$(ratio of CFP-tagged molecules to YFP-tagged molecules $\leq R$).

(B) Analysis of *FR* data for cells coexpressing CFP and α_{1C}-YFP/β_{2a}/$\alpha_{2b}\delta$. Format analogous to (A). *FR*-A_b data plotted as mean ± SD for visual clarity.

(C) Analysis of *FR* data for cells expressing yellow cameleon-2 (YC2) in the Ca^{2+}-free state. Format analogous to (A). *FR*-A_b data plotted as mean ± SD for visual clarity.

(D) Table of $K_{d,EFF}$ and FR_{max} values from fits of measured *FR*.

(E) Analysis of *FR* data for cells coexpressing CaM_{WT}-CFP and β_{2a}-YFP (left) or β_{2a}-CFP and α_{1C}-YFP/$\alpha_{2b}\delta$. Format identical to upper panel of (A).

(F) Coarse triangulation of key channel landmarks. Attached CFP and YFP fluorophores are not shown.

Figure 5A shows the application of such analysis to the pairing of α_{1C}-YFP and CaM_{WT}-CFP. The upper *FR*-A_b plot indicates a robust fit of the binding model to data, with *FR* rising from 1 at $A_b \sim 0$ toward an FR_{max} of 2.9 at $A_b = 1$. Shown below are the distributions of the relative numbers of CaM_{WT}-CFP and α_{1C}-YFP molecules (N_D and N_A, respectively) and the corresponding molar expression ratio of CaM_{WT}-CFP to α_{1C}-YFP molecules (N_D/N_A). The large cell-to-cell variability of this molar expression ratio ensured exploration of nearly the full range of fractional occupancies (A_b). By contrast, control cells coexpressing CFP and α_{1C}-YFP (Figure 5B) give rise to clustering of *FR*-A_b data at $A_b \sim 0$ with an *FR* ~ 1 despite a similar 25-fold distribution of N_D/N_A ratios. Hence, the wide variation of molar expression ratios of α_{1C}-YFP and CaM_{WT}-CFP would not, in itself, cause artifactual elevation of *FR* above unity. Another revealing case involves cells expressing yellow cameleon-2 (Figure 5C), for which the *FR* data congregated at $A_b \sim 1$, as expected for a molecule incorporating both CFP and YFP in a fixed 1:1 stoichiometry. This clustering at $A_b \sim 1$ further supported the accuracy of the A_b estimations produced by our model. Interestingly, the N_A/N_D ratios for yellow cameleon-2 are concentrated at ~ 1, arguing strongly that estimates of relative N_A and N_D in our model are related by a single constant of proportionality to the actual numbers of acceptor and donor molecules.

We extended this analysis to all of our FRET pairs. A summary table of the parameters resulting from these fits is shown in Figure 5D. FR_{max} values for α_{1C}-YFP coexpressed with CaM_{WT}-CFP matched those for α_{1C}-YFP with CaM_{MUT}-CFP, further emphasizing that the detected association entails an authentic Ca^{2+}-independent interaction. Interestingly, whereas FR_{max} values for the different channels were all ~ 3 (equal to the *FR* measured for Ca^{2+}-free yellow cameleon-2), $K_{d,EFF}$ varied substantially. This suggests that the relative affinities for apoCaM are different, while the binding sites are positioned similarly. Interestingly, the rank order of CaM_{MUT} $K_{d,EFF}$ values for the various channel types (Figure 5D; $K_{d,EFF}$ [α_{1E}] $<$ $K_{d,EFF}$ [α_{1C}] $<$ $K_{d,EFF}$ [α_{1A}]) matches that of Ca^{2+}-CaM binding affinities for the corresponding IQ-like domains, as judged by semiquantitative gel-mobility shift assays (Pate et al., 2000; Peterson et al., 1999). One interpretation for this finding is that, despite having the appearance of a purely Ca^{2+}-dependent CaM binding site, the IQ-like domain actually contributes one of multiple ligands forming an apoCaM binding pocket, akin to what has been described for glycogen phosphorylase b kinase and *Bordetella pertussis* adenyl cyclase (Jurado et al., 1999). Such a model could explain recent indirect

evidence that CaM forms a ternary complex with the IQ domain and a separate upstream region when all three constituents are incubated in 100 nM Ca^{2+} (Mouton et al., 2001). FR_{max} values corresponding to association of β_{2a} with CaM_{WT} and α_{1C} with β_{2a} were similar (Figures 5D and 5E). In the case of FRET between labeled α_{1C} and β_{2a} subunits, measured *FR*s were predominantly equal to FR_{max} (Figure 5E), fitting with previous findings that membrane targeting of α_{1C} requires β_{2a} association (Bichet et al., 2000).

Finally, determination of FR_{max} values enabled initial estimates of relative interfluorophore distances (see Experimental Procedures). This formed the basis for the triangle in Figure 5F, which proposes the relative arrangement of key landmarks on the cytoplasmic aspect of the channel: the auxiliary β_{2a} subunit, the α_{1C} carboxyl tail just distal to the IQ site, and preassociated CaM. Labeled CaM and α_{1C} supported an FR_{max} of $\sim$3, which corresponds to an interfluorophore distance of $\sim$60 Å provided that we assume the interfluorophore orientations are sufficiently randomized. The pairing of labeled β_{2a} with either labeled CaM_{WT} or α_{1C} yielded the same FR_{max} of 1.2, corresponding to a comparatively larger interfluorophore distance of about 90 Å. Although there are critical caveats that challenge the reliability of such distance calculations (see Discussion), it is interesting to consider the relative dimensions of the triangle. In favorable instances, these dimensions may prove useful in establishing first-order physical constraints on the organization of a Ca^{2+} channel complex.

Discussion

Ca^{2+}-dependent feedback regulation of L-type and P/Q-type Ca^{2+} channels is mediated by interaction of Ca^{2+}-CaM with the IQ-like domain on the α_1 pore-forming subunit carboxyl tail (DeMaria et al., 2001; Peterson et al., 1999; Qin et al., 1999; Zuhlke et al., 1999). It has been further postulated that apoCaM, rather than being a soluble cytoplasmic entity, may be preassociated with these channels in a manner that could ensure selectivity for local Ca^{2+} signals (DeMaria et al., 2001; Peterson et al., 1999; Zuhlke et al., 1999). Unfortunately, recent in vitro work testing this unorthodox proposal has provided contradictory results (Ivanina et al., 2000; Pate et al., 2000; Peterson et al., 1999; Pitt et al., 2001; Qin et al., 1999; Romanin et al., 2000; Zuhlke et al., 1999). Unravelling this controversy is central to understanding how Ca^{2+}-dependent regulation of Ca^{2+} channels directs such fundamental physiological events as neurotransmitter secretion, short-term synaptic plasticity, and cardiac contraction (Tsien and Tsien, 1990).

Using a practical three-cube FRET method applied to single living cells, we now report clear-cut evidence for Ca^{2+}-independent preassociation of CaM with multiple members of the HVA family of Ca^{2+} channels. Our results establish that CaM_{MUT}-CFP associates within 100 Å of the YFP tagging the α_1 subunit, suggesting that apoCaM preassociates near the IQ-like domain, most probably at a locus on the α_1 pore-forming subunit itself. We focus here on four main lines of discussion. First, we discuss the interrelation between previous in vitro biochemical studies of channel/CaM preassociation and the FRET experiments presented in this report. Second, we compare three-cube FRET to previously established methods for determining steady-state FRET. Third, we explore the correspondence in determining channel/CaM preassociation by three-cube FRET and a complementary donor-dequenching method. Finally, we discuss possible interpretations of the FR_{max} values determined from three-cube FRET measurements.

Roles of Biochemistry- and FRET-Based Assays for Preassociation

Preassociation of apoCaM is an attractive strategy for ensuring rapid and selective modulation by local Ca^{2+}. Although there are relatively few instances where in vitro biochemistry confirms such preassociation (Jurado et al., 1999), the actual prevalence of this mechanism may be far greater, especially for ion channels whose apoCaM interaction might be disrupted during solubilization. Even relatively mild denaturing conditions could disturb formation of a three-dimensional apoCaM binding pocket (see Introduction). Strategies based on FRET circumvent these obstacles by probing interactions between proteins in the natural environment of a living cell, thus providing a critical litmus test for the existence of biologically relevant binding.

When interactions can be preserved in vitro, biochemical assays using purified peptides provide a powerful tool for identifying the specific molecular contacts underlying apoCaM preassociation. Already, some exciting clues have emerged from this approach, although studies conflict in regard to certain key findings. Biochemical screens have primarily targetted amino acid segments in the α_{1C} CI region (Figure 1A) known to be important for Ca^{2+}-dependent modulation of L-type channels (de Leon et al., 1995; Peterson et al., 1999, 2000; Soldatov et al., 1997; Zhou et al., 1997; Zuhlke and Reuter, 1998). One such segment is the IQ-like domain, which binds Ca^{2+}-CaM and is required for Ca^{2+}-dependent modulation (Peterson et al., 1999; Qin et al., 1999; Zuhlke et al., 1999; Zuhlke and Reuter, 1998). It was originally proposed that the IQ-like domain could also be the site for CaM preassociation, since it supported CaM binding at near resting Ca^{2+} concentrations (Zuhlke et al., 1999). Though appealing, this model now seems unlikely because there is no evidence that an IQ peptide could alone interact with CaM_{MUT} (Pate et al., 2000; Pitt et al., 2001), as required for a genuine preassociation locus. Another group recently described Ca^{2+}-independent binding between CaM and a GST-fusion protein incorporating the entire α_{1C} CI region (Romanin et al., 2000). However, the authors report difficulties replicating this result in all preparations (Romanin et al., 2000), and attempts by other groups using the same or similar experimental approach did not detect appreciable binding unless Ca^{2+} concentrations greater than 100 nM were used (Ivanina et al., 2000; Peterson et al., 1999; Qin et al., 1999). A short segment just upstream of the IQ domain was found to interact with CaM at low levels of Ca^{2+} (50–100 nM) approximating those found in resting cells (Pitt et al., 2001; Romanin et al., 2000), but this segment did not bind with CaM in the absence of Ca^{2+}, nor did it alone bind CaM_{MUT} (Pate et al., 2000; Pitt et al., 2001). In what is arguably the most persuasive in

vitro support for apoCaM binding with α_{1C}, Pitt et al. (2001) demonstrated Ca^{2+}-independent binding of CaM to a second CI region segment even farther upstream of the IQ domain. The authors also report binding of CaM_{MUT} to a GST-fusion protein incorporating a major portion of the CI region, including the IQ domain, when incubated in low levels of Ca^{2+} (Pitt et al., 2001). Despite the exciting implications of these results, they contrast with a previous report that GST-fusion proteins incorporating the entire α_{1C} carboxyl tail did not appreciably bind with CaM_{MUT} regardless of Ca^{2+} (Ivanina et al., 2000). Tests for CaM binding to the α_{1C} intracellular loops were also inconsistent (Ivanina et al., 2000; Pitt et al., 2001), although there does appear to be significant Ca^{2+}-dependent binding of CaM to the α_{1C} amino terminus (Ivanina et al., 2000).

These differing results make it difficult to draw firm conclusions about the molecular determinants of apoCaM-channel preassociation. Nonetheless, if we focus exclusively on the positive results of CaM binding to the channel in zero or minimal [Ca^{2+}] (Pitt et al., 2001; Romanin et al., 2000), two points of consensus may be emerging: (1) preassociation of CaM could be coordinated by multiple segments in the CI region, and (2) preassociation could require resting concentrations of Ca^{2+}. In regard to the latter point, our findings that CaM_{MUT} indeed associates with the channel complex would indicate that the requirement for 50–100 nM [Ca^{2+}] does not reflect a need for Ca^{2+} activation of CaM, since CaM_{MUT} does not bind Ca^{2+} over the physiological range (Xia et al., 1998). Instead, resting levels of Ca^{2+} may be transiently needed to allow proper folding of a channel binding pocket for apoCaM (Pitt et al., 2001; Romanin et al., 2000). It will be essential for future work to test these initial points of consensus using a combination of FRET and biochemical experiments, in which mutations that disrupt binding in vitro should result in a corresponding loss of FRET in living cells.

Comparison of Three-Cube FRET to Other Methods for Determining FRET

Three-cube FRET is by no means the only way to measure steady-state CFP/YFP FRET, but many of the existing methods (Selvin, 1995) are not easily adapted into microscope-based assays of fluorescent proteins expressed in single living cells. Measurements of fluorescence lifetime (Harpur et al., 2001), for example, require specialized light sources and detectors capable of quantifying the nanosecond lifetimes of GFP variants. The methods that may be most readily tailored for standard fluorescence microscopes entail measurements of relative emission intensities of the CFP and/or YFP using commonly available optical filters to select for specific excitation and emission wavelengths. Here, we review selected examples of this group of FRET detection methods and highlight some of the special advantages of our three-cube FRET algorithm for studying channel/CaM preassociation.

The simplest approach is to compute the ratio of the YFP/CFP emission peaks at ~535 nm to ~480 nm (Miyawaki et al., 1997). Though this method is ideal for assessing dynamic FRET, it is poorly suited for detecting steady-state FRET in single cells because variable expression of CFP- and YFP-tagged molecules (e.g., Figure 5A) will change this ratio, even in the absence of interaction. More sophisticated strategies account for variable fluorophore concentrations using multiple excitation and emission wavelengths. One class of these emphasizes donor quenching by FRET. For example, FCET (Tron et al., 1984), developed for flow cytometry, provides a quantitative readout of $E \times D_b$, where E is the intrinsic FRET efficiency between associated donor- and acceptor-tagged molecules, and D_b is the fraction of donor-tagged molecules that are preassociated with acceptors. Two features may reduce sensitivity in challenging signal-to-noise regimes, such as with labeled Ca^{2+} channels in single cells. First, determination of $E \times D_b$ involves a calculated constant α, relating enhanced acceptor emission to quenched donor emission. α may not correct for optical peculiarities inherent to the specific system used to determine $E \times D_b$, and these figure increasingly with weaker signals. Second, the emphasis on donor quenching requires precise quantification of emission by CFP, which is considerably dimmer than YFP (Patterson et al., 2001). Another algorithm emphasizing donor quenching measures FRET as FRETN $= E \times D_b/F_A$ (equations 9 and 29 in Gordon et al. [1998]). FRETN involves a calculated G factor, much like the α in FCET. In addition, FRETN could prove particularly insensitive in channel/CaM preassociation experiments, because of the F_A term in the denominator of FRETN. Since there are far fewer channels than CaM molecules (Figure 5A), CFP must be fused to the channel to maximize D_b and favor detection of FRET, seen as FRETN elevation above zero. F_A would then reflect emission from directly excited CaM-YFP. The large excess of CaM-YFP (Figure 5A) would thereby drive FRETN $\rightarrow$ 0, diminishing the resolving power of this method.

Another class of strategies accounting for variable fluorophore levels focuses on sensitized acceptor emission (Selvin, 1995). Clegg (1992) articulated general methods for quantifying sensitized emission, involving curve-fitting algorithms applied to complete emission spectra of fluorophores in solution. Our three-cube FRET method transforms this framework into the setting of three filter-cube determinations performed on single cells with a standard epifluorescence microscope. Moreover, three-cube FRET explicitly establishes and implements key simplifications for optical dissection permitted by the CFP/YFP pair (Figure 2A). These simplifications enable *FR* to be computed entirely with experimentally determined factors that completely correct for optical peculiarities of the microscope system. In addition, the focus on sensitized YFP emission favors sensitive detection of FRET because YFP is much brighter than CFP (Patterson et al., 2001). A distinct advantage of three-cube FRET is that it explicitly accounts for partial binding of donor/acceptor molecules, thereby permitting extraction of relative affinity parameters (Figure 5). To our knowledge, the ratiometric, FCET, and FRETN approaches have not incorporated such a capability. Finally, three-cube FRET can be generalized to other novel fluorophore pairs, such as GFP/DsRed or CFP/DsRed (Moon et al., 2001).

A remaining strategy accounting for variable fluorophore expression requires selective destruction of donor or acceptor molecules. One proven example of this

method for the CFP/YFP pair is donor dequenching (Miyawaki and Tsien, 2000). Here, CFP emission is recorded before and after strong illumination that selectively photobleaches YFP but spares CFP, enabling direct determination of $E \times D_b$ (equation 3, Experimental Procedures). Despite its simplicity and directness, CFP dequenching has some limitations when compared with three-cube FRET. First, the destructive nature of the process precludes FRET measurements before and after biological manipulation of the system. Second, in experiments described below, CFP dequenching proved much slower than three-cube FRET, requiring 15–30 min of intense illumination to achieve near complete (>90%) YFP photodestruction. Third, YFP destruction entailed collateral photobleaching of other cells in the dish, thus limiting the number of cells (<3) that could be assayed per dish.

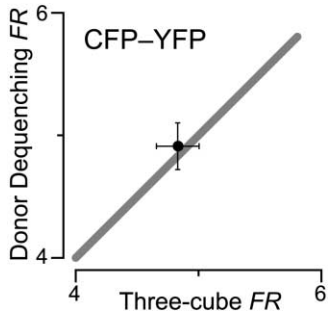

Figure 6. Agreement in Determining FRET within CFP-YFP Dimers by Three-Cube and Donor-Dequenching Methods

Symbol corresponds to mean ± SEM for six cells expressing CFP-YFP, in which *FR* was determined by both donor dequenching and three-cube FRET. The close approximation to the line of identity (gray line) explicitly demonstrates concordance of the methods.

Correspondence in Determining FRET by Three-Cube FRET and Donor Dequenching

Despite these constraints, CFP dequenching may provide the simplest and most practical alternative to three-cube FRET for our experiments and thus provides an important opportunity to independently verify three-cube FRET measurements. Specifically, concordance of these two methods would argue strongly against a number of confounding factors, including the possibility of strong coupling between donor and acceptor fluorophores. We therefore repeated our experiments using CFP dequenching and, for purposes of comparison, "back-calculated" *FR* values from the resulting FRET efficiencies (see below and Experimental Procedures). As an initial verification, we applied donor dequenching to the CFP-YFP concatemer studied earlier in Figure 2B. This approach yielded a back-calculated *FR* of 4.9 ± 0.2 (n = 6), closely matching the value of 5.2 ± 0.1 determined from three-cube FRET (n = 15; Figure 2B). In six cells, we performed both donor dequenching and three-cube measurements, providing head-to-head comparison. When plotted one against the other, *FR* values from the two approaches were indistinguishable from the line of identity (Figure 6).

A second key check on the three-cube method was to apply CFP dequenching to probe apoCaM preassociation with Ca^{2+} channels. Before engaging these experiments, it was necessary to swap the CFP and YFP fluorophores. The reasoning for this change becomes clear by first considering in more detail the rationale for fluorophore attachment in three-cube FRET experiments, where YFP is attached to the channel and CFP is attached to CaM. Since three-cube FRET is based on sensitized YFP emission, *FR* reflects not only the intrinsic FRET efficiency (*E*) when fluorophore-tagged versions of channel subunits and CaM are associated, but also the fraction of YFP-tagged molecules that are preassociated with CFP-tagged molecules (A_b), according to $FR = 1 + [\epsilon_{CFP}(440)/\epsilon_{YFP}(440)] \times E \times A_b$ (equation 2, Experimental Procedures). With YFP fused to the channel, A_b indicates the fraction of channels having preassociated CaM, which is needed to determine the affinity of channel complexes for CaM. If CFP and YFP were swapped, then A_b in this equation would instead correspond to the fraction of CaM molecules associated with channels, an almost meaningless parameter when it comes to determining channel affinity for CaM. Furthermore, given that the number of CaM molecules often far exceeds the number of channels in a cell (Figure 5A), fusing CFP to the channel would result in $A_b \rightarrow 0$ and thus $FR \rightarrow 1$. Fusing YFP to the channel had the added benefit of increasing the effective resolution of FRET to perimembrane regions.

Analogous logic dictates the opposite arrangement of fluorophore attachment in the case of donor dequenching experiments, where CFP must be attached to the channel, and YFP must be attached to CaM. Consider how *FR* is determined via the donor dequenching method. First, by measuring exclusive CFP emission before and after photodestruction of YFP, we determine $E \times D_b$ according to equation 3 (Experimental Procedures), where D_b is the fraction of CFP-tagged molecules that are associated with YFP-tagged molecules. We then back-calculate *FR* by substituting the value of $E \times D_b$ into equation 2, yielding $FR = 1 + [\epsilon_{CFP}(440)/\epsilon_{YFP}(440)] \times E \times D_b$. For this measure of FRET interaction to be relevant, D_b must correspond to the fraction of channels that are associated with CaM; hence, CFP must be attached to the channel. This configuration also ensured that our measurements would benefit from the same perimembrane resolution afforded to three-cube FRET. With this altered configuration, CFP dequenching bore *FR* values (open circles, Figure 5A) that appeared quite similar to those obtained by three-cube FRET. Despite some scatter in the FR-A_b data obtained by both methods, there appeared to be no systematic differences across the range of channel-CaM saturations. Thus, the overall concordance of these two independent methods further supports the existence of genuine FRET coupling between closely associated channel and CaM.

The scatter in the data of Figure 5A, though expected from biological constraints of the experiment, merits discussion. Despite having similar FR_{max} values, the scatter in *FR* data points is comparatively less for yellow cameleon-2 than for the pairing of CaM_{WT}-CFP with α_{1C}-YFP (compare Figure 5A with 5C). This indicates that the noise in Figure 5A is not an intrinsic feature of the three-cube FRET method. Instead, the main reason for the differing levels of scatter is the 10-fold lower expression level of α_{1C}-YFP compared to yellow cameleon-2,

as shown by the corresponding N_A distributions (Figure 5A with 5C, middle). Such diminished expression is an unavoidable biological consequence of producing a large Ca^{2+} channel subunit. Since the three-cube FRET method relies upon sensitized YFP emission, lower expression of the YFP-tagged moiety contributes directly to the increased noise in *FR*. Likewise, for the corresponding donor-dequenching experiments, expression levels for α_{1C}-CFP were 10-fold lower than for yellow cameleon-2. As donor dequenching takes the ratios of CFP fluorescence (equation 3, Experimental Procedures), lower expression of labeled channel also directly increases the noise in *FR* determinations by this method.

Inferring Structure from Differences in FR_{max}

Three-cube FRET measurements enrich our conception of the structures underlying preassociation on multiple levels. These findings answer the important question of whether CaM constitutively preassociates with Ca^{2+} channels in living cells (Figures 3 and 4). *FR* readings significantly greater than 1 can only result from the fluorophores tagging two proteins being separated by less than 100 Å, well within the characteristic dimensions of a Ca^{2+} channel complex (Campbell et al., 1988). These findings further indicate that CaM preassociation requires an interaction with the α_1 subunit itself, as we detected no FRET between CaM_{WT}-CFP and β_{2a}-YFP in the absence of α_1 expression (Figure 3B). CaM_{MUT}-CFP appears to bind to a site that is similarly positioned within L-type, R-type, and P/Q-type channels with respect to the α_1 subunit IQ domain, since the corresponding FR_{max} values are approximately equal (Figure 5D). Finally, the channel landmarks depicted in Figure 5F are all less than ~100 Å apart, thus providing a sense of physical scale for a calcium channel complex.

It is interesting to take an additional step and actually calculate physical distances based on FR_{max} values in order to sketch the dimensions of the protein interactions being studied. This type of analysis would suggest that CaM-CFP is comparatively nearer to the fluorophore tag of α_{1C}-YFP than β_{2a}-CFP (Figure 5F). However, several complicating factors warrant caution when inferring distances and structure from FR_{max} values. First, the wild-type GFP chromophore is encased at the center of a 30 Å wide × 40 Å tall β barrel structure (Yang et al., 1996), indicating that the physical separation between closely apposed GFP chromophores must be at least 30 Å. This limitation places restrictions on the minimum quantifiable distance detectable by CFP/YFP FRET. Interpretation of computed distances is further complicated because FRET reflects the separations between CFP and YFP chromophores, not the proteins to which they are attached. Overall, geometric considerations would indicate that a calculated distance of 60 Å between fluorophores attached to CaM and the IQ domain suggests that CaM preassociates with the channel complex at a site no more than about 100 Å from the IQ site.

Second, it is also well known that changes in R_0, which is needed to compute distance from FR_{max}, can arise from differences in interfluorophore dipole orientation (Selvin, 1995). These orientations are impossible to determine without precise molecular structures. In most cases, including here, distance calculations are greatly simplified by assuming that the fluorophore tags adopt sufficiently randomized orientations during their excited state lifetimes. One must be particularly careful in applying this assumption to bulky fluorophores like CFP or YFP, which have spatial dimensions on the same order as CaM and are likely to be sterically constrained in the close quarters of a channel/CaM interface. For example, it is possible that CaM-CFP and β_{2a}-YFP are actually quite close but that the fluorophore dipoles are misaligned such that FRET coupling is weakened substantially. Smaller fluorophores, such as fluorescein and tetramethylrhodamine, are more likely to have the rotational freedom required to satisfy this assumption (Glauner et al., 1999). The actual impact of nonrandom orientations may be small, since changes in R_0 computed over the large majority of possible orientations result in less than ±30% variation in predicted distances (Van Der Meer et al., 1994), but we nevertheless remain uncertain as to the actual orientations of the flourophores studied here.

Third, given that there appear to be multiple CaM binding sites on α_{1C} (Ivanina et al., 2000; Pitt et al., 2001), it is possible that two or more CaM-CFP molecules simultaneously reside within 100 Å of the YFP attached to α_{1C}. Such coupling with multiple donors, if significant, would alter equation 2 (Experimental Procedures) and the associated calculations of distance. To address this scenario, we considered alternative models for the data in Figure 5 in which two or more CaM-CFP molecules reside within FRET interaction distance of α_{1C}-YFP; however, the distinctions in predicted behavior were too small to be resolved relative to the noise in our data. Thus, we cannot exclude the possibility that multiple CaM-CFP molecules simultaneously associate with a single α_{1C}-YFP, but we also would not expect this possibility to substantially alter our main conclusions.

In summary, although these caveats complicate quantitative interpretation of FRET, it is interesting to consider calculated distances as a first-order gauge of the structures underlying apoCaM preassociation. In favorable scenarios, the errors generated by these caveats would be smaller than the relative distances proposed by the triangle in Figure 5F, and the qualitative features of the model may provide useful initial constraints on the structure of a calcium channel complex. It will be interesting to see if future work with less bulky fluorophores will confirm these relative dimensions.

Conclusions

The presumed raison d'être of apoCaM preassociation in Ca^{2+} channels is that it enables rapid modulation spurred by elevations in local Ca^{2+} (Peterson et al., 1999; Zuhlke et al., 1999). This model requires that apoCaM be preassociated to the channel complex in close proximity to both the pore and the Ca^{2+}-dependent effector site. Our results establish that apoCaM indeed preassociates with the Ca^{2+} channel complex in living cells at a locus that is near the IQ-like domain (within ~100 Å), making preassociation an integral feature of the molecular mechanisms underlying Ca^{2+}-dependent regulation of these channels. In addition, evidence for widespread apoCaM preassociation across Ca^{2+} channel types motivates a renewed search for Ca^{2+}-dependent modula-

tion of gating in other members of the HVA Ca^{2+} channel family.

Experimental Procedures

Subcloning and Mutagenesis

ECFP and EYFP (referred to as CFP and YFP throughout) were PCR amplified from yellow cameleon-2 (Miyawaki et al., 1997) (gift from R.Y. Tsien) and fused to target proteins. The CFP-YFP concatemer linked CFP and YFP with SRAQASNSAVDGTAGPGSIAT. For CaM_{WT}-CFP, CFP was truncated before Gly_{232} and fused to the amino terminus of CaM_{WT} (Peterson et al., 1999) with an AA linker using PCR-mediated overlap extension (Horton et al., 1989); CFP was fused to CaM_{MUT} (Peterson et al., 1999) identically. For three-cube FRET, CFP, YFP, CFP-YFP, CaM_{WT}-CFP, and CaM_{MUT}-CFP were subcloned into pZeoSV2 (Invitrogen), with the weak SV40 promoter and no SV40 replication origin. Using an SS linker, YFP was fused to the carboxyl terminus of $\alpha_{1C}\Delta1671\Delta^*$, a custom α_{1C} ($Ca_V1.2$) with carboxy-terminal truncation before Gly_{1671} (17 residues downstream of IQ-like domain Ile) and no stop codon. Similar α_{1E} ($Ca_V2.3$) and α_{1A} ($Ca_V2.1$) YFP fusions were constructed using custom $\alpha_{1E}\Delta1843\Delta^*$ and $\alpha_{1A}\Delta1930\Delta^*$ truncation constructs. CFP and YFP were attached to the carboxyl terminus of rat brain β_{2a} with the linker GSIAT. All fusion constructs were confirmed by digests, sequencing, spectrofluorimetry, and, where appropriate, electrophysiology.

Electrophysiology

Whole-cell patch-clamp recordings from HEK293 cells were acquired as described (Peterson et al., 1999) 3 days posttransfection by calcium phosphate precipitation with cDNAs encoding α_{1C}-YFP, β_{2a}, $\alpha_{2b}\delta$, and either CaM-CFP or CaM_{MUT}-CFP, both in pcDNA3 (Invitrogen). All electrophysiological and three-cube FRET data are reported as mean ± SEM.

FRET Measurements

HEK293 cells were thinly plated into 3.5 cm culture dishes with integral No. 0 glass coverslip bottoms (MatTek) and transiently transfected with FuGene 6 (Roche Molecular Biochemicals). Three days later, the cells were washed, bathed in HEPES-buffered Tyrode's (pH 7.35), and assessed with a Nikon TE300 Eclipse microscope (40× 1.3 n.a. objective) and custom fluorometer system (University of Pennsylvania Biomedical Instrumentation Group). Excitation light was delivered by a 150 W short-gap Xenon arc-lamp (Optiquip) gated by a computer-controlled shutter (Vincent Associates). Epifluorescence emission from entire individual cells was selected by an image-plane pinhole and measured with an ambient temperature photomultiplier tube (PMT) (30 mm EMI 9124B; Electron Tubes). PMT signals were integrated and filtered (10 kHz) by the fluorimeter and digitized (ITC-18; Instrutech). Shutter control, data acquisition, and dark-current subtraction were controlled by custom MATLAB (MathWorks) software employing DeviceAccess drivers (Bruxton). To remove autofluorescence and background light scatter, averages from individual cells expressing untagged proteins were subtracted from same-day experimental values for each filter cube. The background signals on any given day varied little and signal:background for the FRET cube was >6:1. CFP emission accounted for up to 75% of the signal in the FRET cube but generally was lower because expression of CFP-tagged molecules was attenuated. Three-cube FRET filtercubes (excitation, dichroic, emission, company): CFP (D440/20M, 455DCLP, D480/30M, Chroma); YFP (500RDF25, 525DRLP, 530EFLP, Omega Optical); FRET (440DF20, 455DRLP, 535DF25, Omega Optical).

FR and FRET Efficiency Computation

FRET Ratio (*FR*) is equal to the fractional increase in YFP emission due to FRET and was calculated as

$$FR = \frac{F_{A_D}}{F_A} = \frac{[S_{FRET}\,(DA) - R_{D1} \cdot S_{CFP}\,(DA)]}{R_{A1} \cdot [S_{YFP}\,(DA) - R_{D2} \cdot S_{CFP}\,(DA)]} \quad (1)$$

S_{CUBE}(SPECIMEN) denotes an intensity measurement, where CUBE indicates the filter cube (CFP, YFP, or FRET) and SPECIMEN indicates whether the cell is expressing donor (D; CFP), acceptor (A; YFP), or both (DA). $R_{D1} = S_{FRET}(D)/S_{CFP}(D)$, $R_{D2} = S_{YFP}(D)/S_{CFP}(D)$, and $R_{A1} = S_{FRET}(A)/S_{YFP}(A)$ are predetermined constants from measurements applied to single cells expressing only CFP- or YFP-tagged molecules (see online Supplemental Appendix A1 for complete development of method). Although three-cube FRET does not require that CFP and YFP fusion constructs preserve the spectral features of the unattached fluorophores, similar ratios (Supplemental Table S1) and recorded spectra (data not shown) furnished two indications that the spectral features of the fluorophores were largely unperturbed by fusion. Since *FR* relies on YFP emission, YFP should be attached to the presumed limiting moiety in a given interaction; in most cases, that meant attaching YFP to Ca^{2+} channel subunits and CFP to CaM. Subsequent quantitative calculations based on *FR* relied on a presumed 1:1 interaction stoichiometry. The effective FRET efficiency (E_{EFF}) was determined by

$$E_{EFF} = E \times A_b = (FR - 1)[\epsilon_{YFP}(440)/\epsilon_{CFP}(440)] \quad (2)$$

where E is the intrinsic FRET efficiency when fluorophore-tagged molecules are associated with each other, A_b is the fraction of YFP-tagged molecules that are associated with CFP-tagged molecules, and the bracketed term is the ratio of YFP and CFP molar extinction coefficients scaled for the FRET cube excitation filter (Epe et al., 1983). We determined this ratio to be 0.094 based on maximal extinction coefficients for ECFP and EYFP (Patterson et al., 2001) and excitation spectra measured in our lab. FRET was also assessed by measuring dequenching of donor emission following nearly complete acceptor photodestruction (Miyawaki and Tsien, 2000) by 30 min of strong illumination through a 540AF30 excitation filter. This spared the CFP chromophore in control experiments. Here, the effective FRET efficiency is calculated as

$$E_{EFF} = E \times D_b = [1 - S_{CFP}(DA)_{before}/S_{CFP}(DA)_{after}] \quad (3)$$

where $S_{CFP}(DA)_{before}$ and $S_{CFP}(DA)_{after}$ are CFP emission prior to and following YFP photobleaching, and D_b is the fraction of CFP-tagged molecules that are associated with YFP-tagged molecules (Epe et al., 1983). By tagging Ca^{2+} channel subunits with CFP, CaM with YFP, and measuring E by donor dequenching, we could back calculate an *FR* by substituting E_{EFF} from equation 3 into equation 2, providing independent verification of the three-cube FRET method (Figure 5A).

Estimation of Physical Distance and Binding Affinity

Details of the preassociation model are available in Supplemental Appendix A2; the following describes the representative example of interactions between α_{1C}-YFP and CaM-CFP. With incomplete saturation of α_{1C}-YFP by CaM-CFP, the measured *FR* is discounted from the maximal value (FR_{max}) according to the equation $FR = 1 + A_b\,(FR_{max} - 1)$, where A_b is the fraction of α_{1C}-YFP proteins with an associated CaM-CFP. A_b is given by the 1:1 ligand binding function $A_b = 1/(1 + 2 \times K_d/[D_{free}])$, where K_d is the dissociation constant, $[D_{free}]$ is the concentration of unbound CaM-CFP, and the factor of 2 relates to the fact that CaM-CFP molecules can only bind to α_{1C}-YFP molecules from the cytoplasmic side of the membrane. Using the individual *CFP* and *YFP* cube measurements provided by the three-cube FRET assay, we estimated the relative numbers of CFP- and YFP-tagged proteins, which in turn were employed to compute a relative D_{free}. For each *FR* measurement, we computed a predicted A_b, which in turn was used to calculate $FR_{predicted}$. By minimizing the sum of the squared errors $(FR - FR_{predicted})^2$ across many cells, we fixed the two free parameters, FR_{max} and the "effective" dissociation constant, or $K_{d,EFF}$. When calculated from FR_{max}, $E = (FR_{max} - 1)[\epsilon_{YFP}(440)/\epsilon_{CFP}(440)]$ provided an estimate of CFP-YFP separation, R, using the standard equation $R = R_0(E^{-1} - 1)^{1/6}$ (Selvin, 1995), with $R_0 = 49$ Å (Patterson et al., 2000).

SDS-PAGE and Immunoblot Analysis

HEK293 cells were harvested and lysed 3 days after calcium-phosphate transfection. Protein concentrations were determined by the bicinchoninic acid assay (Pierce) using BSA (Sigma) as a standard. Aliquots (50 μg) of lysates were incubated in 5 mM EGTA for 30 min on ice, resolved on 12.5% SDS-PAGE, and electroblotted to Hybond membrane (Amersham) as described (Towbin et al., 1979), with purified recombinant CaM proteins (DeMaria et al., 2001) as positive

controls. Detection of endogenous CaM was optimized by cooled transfer at 25V for 16 hr in 50 mM potassium phosphate (pH 7.0), followed immediately by rocking in 0.2% (v/v; freshly prepared in transfer buffer) glutaraldehyde (Sigma) for 20 min at room temperature. Proteins were detected using monoclonal anti-GFP (Covance) or anti-CaM (Research Diagnostics) antibodies and horseradish peroxidase-conjugated secondary antibody (Sigma), visualized with enhanced chemiluminescence (Amersham).

Acknowledgments

We thank Devi Rathod, Rebecca Alvania, Tracy Morrison, and Daniel Moon for technical support and helpful discussion; Aldrin Gomes for advice on CaM Western blots; and Scot Kuo for helpful comments on the manuscript. This work was supported by a Whitaker Foundation Graduate Fellowship (M.G.E.) and grants from the American Heart Association and National Institutes of Health (D.T.Y.).

Received May 22, 2001; revised August 22, 2001.

References

Bichet, D., Cornet, V., Geib, S., Carlier, E., Volsen, S., Hoshi, T., Mori, Y., and De Waard, M. (2000). The I-II loop of the Ca^{2+} channel α_1 subunit contains an endoplasmic reticulum retention signal antagonized by the β subunit. Neuron *25*, 177–190.

Brehm, P., and Eckert, R. (1978). Calcium entry leads to inactivation of calcium channel in Paramecium. Science *202*, 1203–1206.

Campbell, K.P., Leung, A.T., and Sharp, A.H. (1988). The biochemistry and molecular biology of the dihydropyridine-sensitive calcium channel. Trends Neurosci. *11*, 425–430.

Chao, S.H., Suzuki, Y., Zysk, J.R., and Cheung, W.Y. (1984). Activation of calmodulin by various metal cations as a function of ionic radius. Mol. Pharmacol. *26*, 75–82.

Chien, A.J., Zhao, X., Shirokov, R.E., Puri, T.S., Chang, C.F., Sun, D., Rios, E., and Hosey, M.M. (1995). Roles of a membrane-localized β subunit in the formation and targeting of functional L-type Ca^{2+} channels. J. Biol. Chem. *270*, 30036–30044.

Clegg, R.M. (1992). Fluorescence resonance energy transfer and nucleic acids. Methods Enzymol. *211*, 353–388.

de Leon, M., Wang, Y., Jones, L., Perez-Reyes, E., Wei, X., Soong, T.W., Snutch, T.P., and Yue, D.T. (1995). Essential Ca^{2+}-binding motif for Ca^{2+}-sensitive inactivation of L- type Ca^{2+} channels. Science *270*, 1502–1506.

DeMaria, C.D., Soong, T.W., Alseikhan, B.A., Alvania, R.S., Agnew, W.S., and Yue, D.T. (2001). Calmodulin bifurcates the local Ca^{2+} signal that modulates P/Q-type Ca^{2+} channels. Nature *411*, 484–489.

Epe, B., Steinhäuser, K.G., and Woolley, P. (1983). Theory of measurement of Förster-type energy transfer in macromolucules. Proc. Natl. Acad. Sci. USA *80*, 2579–2583.

Glauner, K.S., Mannuzzu, L.M., Gandhi, C.S., and Isacoff, E.Y. (1999). Spectroscopic mapping of voltage sensor movement in the Shaker potassium channel. Nature *402*, 813–817.

Gordon, G.W., Berry, G., Liang, X.H., Levine, B., and Herman, B. (1998). Quantitative fluorescence resonance energy transfer measurements using fluorescence microscopy. Biophys. J. *74*, 2702–2713.

Harpur, A.G., Wouters, F.S., and Bastiaens, P.I. (2001). Imaging FRET between spectrally similar GFP molecules in single cells. Nat. Biotechnol. *19*, 167–169.

Horton, R.M., Hunt, H.D., Ho, S.N., Pullen, J.K., and Pease, L.R. (1989). Engineering hybrid genes without the use of restriction enzymes: gene splicing by overlap extension. Gene *77*, 61–68.

Ivanina, T., Blumenstein, Y., Shistik, E., Barzilai, R., and Dascal, N. (2000). Modulation of L-type Ca^{2+} channels by $G_{\beta\gamma}$ and calmodulin via interactions with N and C termini of α_{1C}. J. Biol. Chem. *275*, 39846–39854.

Janetopoulos, C., Jin, T., and Devreotes, P. (2001). Receptor-mediated activation of heterotrimeric G-proteins in living cells. Science *291*, 2408–2411.

Jurado, L.A., Chockalingam, P.S., and Jarrett, H.W. (1999). Apocalmodulin. Physiol. Rev. *79*, 661–682.

Lee, A., Wong, S.T., Gallagher, D., Li, B., Storm, D.R., Scheuer, T., and Catterall, W.A. (1999). Ca^{2+}/calmodulin binds to and modulates P/Q-type calcium channels. Nature *399*, 155–159.

Miyawaki, A., and Tsien, R.Y. (2000). Monitoring protein conformations and interactions by fluorescence resonance energy transfer between mutants of green fluorescent protein. Methods Enzymol. *327*, 472–500.

Miyawaki, A., Llopis, J., Heim, R., McCaffery, J.M., Adams, J.A., Ikura, M., and Tsien, R.Y. (1997). Fluorescent indicators for Ca^{2+} based on green fluorescent proteins and calmodulin. Nature *388*, 882–887.

Moon, D.L., Erickson, M.G., and Yue, D.T. (2001). DsRed as a FRET partner with EGFP and ECFP. Biophys. J. *80*, 362a.

Mouton, J., Feltz, A., and Maulet, Y. (2001). Interactions of calmodulin with two peptides derived from the C-terminal cytoplasmic domain of the $Ca_v1.2$ Ca^{2+} channel provide evidence for a molecular switch involved in Ca^{2+}-induced inactivation. J. Biol. Chem. *276*, 22359–22367.

Pate, P., Mochca-Morales, J., Wu, Y., Zhang, J.Z., Rodney, G.G., Serysheva, II, Williams, B.Y., Anderson, M.E., and Hamilton, S.L. (2000). Determinants for calmodulin binding on voltage-dependent Ca^{2+} channels. J. Biol. Chem. *275*, 39786–39792.

Patterson, G.H., Piston, D.W., and Barisas, B.G. (2000). Forster distances between green fluorescent protein pairs. Anal. Biochem. *284*, 438–440.

Patterson, G., Day, R.N., and Piston, D. (2001). Fluorescent protein spectra. J. Cell. Sci. *114*, 837–838.

Peterson, B.Z., DeMaria, C.D., Adelman, J.P., and Yue, D.T. (1999). Calmodulin is the Ca^{2+} sensor for Ca^{2+}-dependent inactivation of L-type calcium channels. Neuron *22*, 549–558.

Peterson, B.Z., Lee, J.S., Mulle, J.G., Wang, Y., de Leon, M., and Yue, D.T. (2000). Critical determinants of Ca^{2+}-dependent inactivation within an EF-hand motif of L-type Ca^{2+} channels. Biophys. J. *78*, 1906–1920.

Pitt, G.S., Zuhlke, R.D., Hudmon, A., Schulman, H., Reuter, H., and Tsien, R.W. (2001). Molecular basis of CaM tethering and Ca^{2+}-dependent inactivation of L-type Ca^{2+} channels. J. Biol. Chem. *276*, 30794–30802.

Qin, N., Olcese, R., Bransby, M., Lin, T., and Birnbaumer, L. (1999). Ca^{2+}-induced inhibition of the cardiac Ca^{2+} channel depends on calmodulin. Proc. Natl. Acad. Sci. USA *96*, 2435–2438.

Rhoads, A.R., and Friedberg, F. (1997). Sequence motifs for calmodulin recognition. FASEB J. *11*, 331–340.

Rodney, G.G., Moore, C.P., Williams, B.Y., Zhang, J.Z., Krol, J., Pedersen, S.E., and Hamilton, S.L. (2000). Calcium binding to calmodulin leads to an N-terminal shift in its binding site on the ryanodine receptor. J. Biol. Chem. *276*, 2069–2074.

Romanin, C., Gamsjaeger, R., Kahr, H., Schaufler, D., Carlson, O., Abernethy, D.R., and Soldatov, N.M. (2000). Ca^{2+} sensors of L-type Ca^{2+} channel. FEBS Lett. *487*, 301–306.

Schumacher, M.A., Rivard, A.F., Bachinger, H.P., and Adelman, J.P. (2001). Structure of the gating domain of a Ca^{2+}-activated K^+ channel complexed with Ca^{2+}/calmodulin. Nature *410*, 1120–1124.

Selvin, P.R. (1995). Fluorescence resonance energy transfer. Methods Enzymol. *246*, 300–334.

Siegel, R.M., Frederiksen, J.K., Zacharias, D.A., Chan, F.K., Johnson, M., Lynch, D., Tsien, R.Y., and Lenardo, M.J. (2000). Fas preassociation required for apoptosis signaling and dominant inhibition by pathogenic mutations. Science *288*, 2354–2357.

Soldatov, N.M., Zuhlke, R.D., Bouron, A., and Reuter, H. (1997). Molecular structures involved in L-type calcium channel inactivation. Role of the carboxyl-terminal region encoded by exons 40-42 in α_{1C} subunit in the kinetics and Ca^{2+} dependence of inactivation. J. Biol. Chem. *272*, 3560–3566.

Stryer, L., and Haugland, R.P. (1967). Energy transfer: a spectroscopic ruler. Proc. Natl. Acad. Sci. USA *58*, 719–726.

Towbin, H., Staehelin, T., and Gordon, J. (1979). Electrophoretic

transfer of proteins from polyacrylamide gels to nitrocellulose sheets: procedure and some applications. Proc. Natl. Acad. Sci. USA *76*, 4350–4354.

Tron, L., Szollosi, J., Damjanovich, S., Helliwell, S.H., Arndt-Jovin, D.J., and Jovin, T.M. (1984). Flow cytometric measurement of fluorescence resonance energy transfer on cell surfaces. Quantitative evaluation of the transfer efficiency on a cell-by-cell basis. Biophys. J. *45*, 939–946.

Tsien, R.W., and Tsien, R.Y. (1990). Calcium channels, stores, and oscillations. Annu. Rev. Cell. Biol. *6*, 715–760.

Van Der Meer, B.W., Coker, G., and Chen, S.-Y.S. (1994). Resonance Energy Transfer: Theory and Data (New York: VCH Publishers).

Vanderklish, P.W., Krushel, L.A., Holst, B.H., Gally, J.A., Crossin, K.L., and Edelman, G.M. (2000). Marking synaptic activity in dendritic spines with a calpain substrate exhibiting fluorescence resonance energy transfer. Proc. Natl. Acad. Sci. USA *97*, 2253–2258.

Xia, X.M., Fakler, B., Rivard, A., Wayman, G., Johnson-Pais, T., Keen, J.E., Ishii, T., Hirschberg, B., Bond, C.T., Lutsenko, S., et al. (1998). Mechanism of calcium gating in small-conductance calcium-activated potassium channels. Nature *395*, 503–507.

Yang, F., Moss, L.G., and Phillips, G.N. (1996). The molecular structure of green fluorescent protein. Nat. Biotechnol. *14*, 1246–1251.

Zhou, J., Olcese, R., Qin, N., Noceti, F., Birnbaumer, L., and Stefani, E. (1997). Feedback inhibition of Ca^{2+} channels by Ca^{2+} depends on a short sequence of the C terminus that does not include the Ca^{2+}-binding function of a motif with similarity to Ca^{2+}-binding domains. Proc. Natl. Acad. Sci. USA *94*, 2301–2305.

Zuhlke, R.D., and Reuter, H. (1998). Ca^{2+}-sensitive inactivation of L-type Ca^{2+} channels depends on multiple cytoplasmic amino acid sequences of the α_{1C} subunit. Proc. Natl. Acad. Sci. USA *95*, 3287–3294.

Zuhlke, R.D., Pitt, G.S., Deisseroth, K., Tsien, R.W., and Reuter, H. (1999). Calmodulin supports both inactivation and facilitation of L-type calcium channels. Nature *399*, 159–162.